Available online at www.sciencedirect.com
SCIENCE DIRECT®
Journal of Solid State Chemistry 177 (2004) 3499–3504
JOURNAL OF SOLID STATE CHEMISTRY
http://elsevier.com/locate/jssc

Synthesis, crystal structure, and magnetic properties of new layered hexagonal perovskite $Ba_8Ta_4Ru_{8/3}Co_{2/3}O_{24}$

E.M. Kopnin,[a,*] A.A. Belik,[a,1] R.V. Shpanchenko,[b] E.V. Antipov,[b] F. Izumi,[a] E. Takayama-Muromachi,[a] and J. Hadermann[c]

[a] *Advanced Materials Laboratory, National Institute for Material Science, 1-1 Namiki, Tsukuba, Ibaraki 305-0044, Japan*
[b] *Department of Chemistry, Moscow State University, Moscow, Leninskie Gory 119992, Russia*
[c] *EMAT, University of Antwerp (RUCA), Groenenborgerlaan 171, 2020 Antwerp, Belgium*

Received 16 December 2003; received in revised form 9 April 2004; accepted 18 April 2004

Available online 11 August 2004

Abstract

A new hexagonal perovskite-type oxide $Ba_8Ta_4Ru_{8/3}Co_{2/3}O_{24}$ was synthesized by the solid-state method at 1573 K and characterized by electron diffraction (ED), time-of-flight (TOF) neutron powder diffraction, and magnetic susceptibility. Structure parameters of $Ba_8Ta_4Ru_{8/3}Co_{2/3}O_{24}$ were refined by the Rietveld method from the TOF neutron powder diffraction data on the basis of space group $P6_3/mcm$ and lattice parameters $a = 10.0075(1)$ Å and $c = 18.9248(2)$ Å as obtained from the ED data ($Z = 3$). The crystal structure of $Ba_8Ta_4Ru_{8/3}Co_{2/3}O_{24}$ consists of 8-layered $(cchc)_2$ close-packed stacking of BaO_3 layers along the c-axis. Corner-shared octahedra are filled by Ta only and face-shared octahedra are statistically occupied by Ru, Co, and vacancies. Similar compounds $Ba_8Ta_4Ru_{8/3}M_{2/3}O_{24}$ with M = Ni and Zn were also prepared. Magnetic susceptibility measurements showed no magnetic ordering down to 5 K.

Keywords: Hexagonal perovskites; Ruthenium oxides; Electron diffraction; Superstructure; Neutron diffraction; Crystal structure; Cation distribution

1. Introduction

Crystal structures of complex hexagonal perovskites contain close-packed AO_3 (A = Sr, Ba, and La) layers along the c-axis of the unit cell. The interstices are usually occupied by octahedrally coordinated cations with high formal oxidation states and form chains of face-shared octahedra (FSO). These chains are connected by corner-shared octahedra (CSO). The electrostatic repulsion of cations in FSO can be compensated in different ways, e.g., (1) by formation of metal–metal bonds and (2) by introduction of cation vacancies or cations with small formal charges in FSO [1–3]. Numerous compounds belonging to B-deficient layered perovskites $A_nB_{n-1}O_{3n}$ with different n ($n \geqslant 3$) were reported in the literature. There are two different structural types in this series. They can be described using the different stacking sequences. First sequence can be generally expressed as $(hhc\ldots c)$ and the structures contain completely empty B-site between two face-sharing layers [4–21]. In the second case the positions in FSO are partially occupied and the stacking sequence can be written as $(hc\ldots c)$ [12, 22–25]. In $Ba_8Ta_4Ti_3O_{24}$ and $Ba_8Nb_4Ti_3O_{24}$, e.g., the positions in FSO were found to be occupied mainly by Ti^{4+} ions and partially vacant [12]. The crystal structures of these two compounds were given in space group $P6_3/mmc$ with $a_{sub} \approx 5.8$ Å and $c_{sub} \approx 19$ Å. However, they have recently been reinvestigated taking into account a superstructure ($a = \sqrt{3} \times a_{sub}$ and $c = c_{sub}$; space group $P6_3/mcm$) observed by electron diffraction (ED) [22,24]. The successful synthesis of $Ba_8Ta_6NiO_{24}$ demonstrated that Ni^{2+} ions with the lower oxidation state than Ti^{4+} ions also can occupy the metal positions in FSO [23].

*Corresponding author. Present address: Pirelli Labs SpA, C2171, Viale Sarca 222, I-20126 Milan, Italy. Fax: +39-02-6442-9431.
E-mail address: evgeny.kopnin@pirelli.com (E.M. Kopnin).
[1] Present address: Institute for Chemical Research, Kyoto University, Uji, Kyoto-fu 611-0011, Japan.

0022-4596/$ - see front matter © 2004 Elsevier Inc. All rights reserved.
doi:10.1016/j.jssc.2004.04.032

In this work, we have synthesized new perovskite-type oxides with 8-layered hexagonal structures, $Ba_8Ta_4Ru_{8/3}M_{2/3}O_{24}$ (M = Co, Ni, and Zn), and characterized them by X-ray powder diffraction (XRD) and magnetic susceptibility measurements. We have also found a superstructure ($a = 10.008$ Å and $c = 18.925$ Å) for $Ba_8Ta_4Ru_{8/3}Co_{2/3}O_{24}$ by ED and refined structure parameters of this compound from time-of-flight (TOF) neutron powder diffraction data adopting the superstructure model.

2. Experimental section

$Ba_8Ta_4Ru_{8/3}M_{2/3}O_{24}$ (M = Co, Ni, and Zn) were prepared by the solid-state method from mixtures of $BaCO_3$, Ta_2O_5, RuO_2, and MO (M = Co, Ni, and Zn) with an amount-of-substance ratio of 12:3:4:1. All precursors were preliminary dried at 573–673 K. The mixtures were annealed at 1273 K for 50 h, reground, pressed into pellets, and allowed to react at 1473 K for 100 h and 1573 K (1673 K in the case of M = Ni) for 200 h in an electric furnace with 2–3 intermediate grindings. The samples were finally cooled in the furnace. They were characterized by XRD using a Philips PW 1800 diffractometer with Cu$K\alpha$ radiation (2θ range: 10–80°, step width: 0.02°, counting time per step: 1 s). The XRD data showed $Ba_8Ta_4Ru_{8/3}M_{2/3}O_{24}$ (M = Co, Ni, and Zn) to contain a trace amount of $Ba_3MRu_2O_9$ [26–30] and a few very weak unidentified reflections. Reflections in the XRD patterns of $Ba_8Ta_4Ru_{8/3}M_{2/3}O_{24}$ (M = Co, Ni, and Zn) could be indexed in a hexagonal system with lattice parameters of $a = 5.7753(7)$ Å and $c = 18.926(4)$ Å for M = Co, $a = 5.804(1)$ Å and $c = 18.994(4)$ Å for M = Ni, and $a = 5.7810(6)$ Å and $c = 18.944(4)$ Å for M = Zn. In the present study, the crystal structure of $Ba_8Ta_4Ru_{8/3}Co_{2/3}O_{24}$ has been investigated in details by ED and TOF neutron powder diffraction.

For transmission electron microscopy observations, $Ba_8Ta_4Ru_{8/3}Co_{2/3}O_{24}$ was crushed in ethanol and deposited on copper grids covered with a holey carbon film. Selected-area ED patterns were taken on a Phillips CM20 electron microscope.

TOF neutron powder diffraction data of $Ba_8Ta_4Ru_{8/3}Co_{2/3}O_{24}$ were collected at room temperature on the powder diffractometer Sirius at the pulsed spallation neutron facility KENS. About 600 mg of the sample was loaded into a V holder, which was slowly rotated during the measurement. An array of 160 position-sensitive detectors (PSDs) installed in a backward bank with a 2θ range from 150° to 170° was used to measure the intensity data. Incident neutron spectra were monitored with an ^{3}He monitor counter. Differences in efficiency between the PSDs were corrected with intensity data taken in a separate measurement of incoherent scattering from V. The resultant TOF neutron powder diffraction data in a d range from 0.45 to 2.5 Å were analyzed by the Rietveld method with RIETAN-TN [31]. A composite background function, i.e., a 14th-order Legendre polynomial multiplied by a smoothed incident spectrum, was fit to the background. Bound coherent scattering lengths, b_c, used for the Rietveld refinement were 5.07 fm (Ba), 6.91 fm (Ta), 7.03 fm (Ru), 2.49 fm (Co), and 5.803 fm (O) [32]. Isotropic atomic displacement parameters, U, with the isotropic Debye–Waller factor formulated as $\exp(-8\pi^2 U \sin^2\theta/\lambda^2)$ were assigned to all the sites.

Magnetic susceptibilities, χ, of $Ba_8Ta_4Ru_{8/3}Co_{2/3}O_{24}$ and $Ba_8Ta_4Ru_{8/3}Zn_{2/3}O_{24}$ were measured on a DC SQUID magnetometer (Quantum Design, MPMS) between 5 and 300 K in an applied field of 100 Oe ($1\,\text{Oe} = [10^3/4\pi]\,\text{A m}^{-1}$) under both zero-field-cooled (ZFC) and field-cooled (FC) conditions.

3. Results

Fig. 1 presents plots of χ^{-1} (ZFC curves) against temperature, T, for $Ba_8Ta_4Ru_{8/3}Co_{2/3}O_{24}$ and $Ba_8Ta_4Ru_{8/3}Zn_{2/3}O_{24}$. No noticeable difference was found between the curves measured under the ZFC and FC conditions. The $\chi^{-1}(T)$ data in the temperature range 100–300 K were fitted to the Curie–Weiss law plus the temperature-independent term (χ_0) using the following equation:

$$\chi(T) = \chi_0 + C/(T-\theta), \tag{1}$$

where C is the Curie constant, and θ is the Weiss constant.

The fitted parameters were $C = 0.832(15)\,\text{cm}^3\,\text{K/mol}$, $\theta = -32(2)$ K, and $\chi_0 = 1.51(3)\times10^{-3}\,\text{cm}^3/\text{mol}$ for $Ba_8Ta_4Ru_{8/3}Zn_{2/3}O_{24}$ and $C = 2.21(7)\,\text{cm}^3\,\text{K/mol}$, $\theta = -23(3)$ K, and $\chi_0 = 2.57(16)\times10^{-3}\,\text{cm}^3/\text{mol}$ for $Ba_8Ta_4Ru_{8/3}Co_{2/3}O_{24}$. The negative Weiss constant supports the idea that some antiferromagnetic Ru^{4+}–O–Ru^{4+}

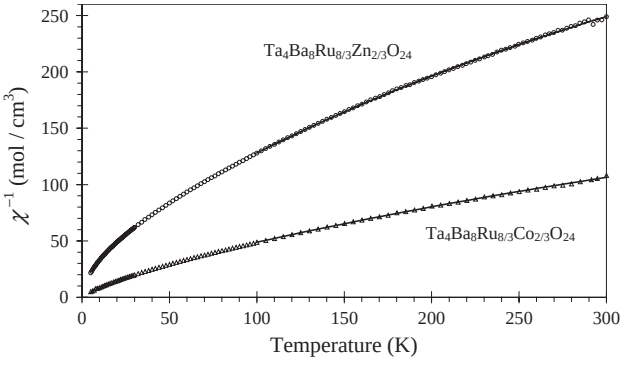

Fig. 1. Inverse magnetic susceptibilities, χ^{-1}, plotted against temperature for $Ba_8Ta_4Ru_{8/3}Co_{2/3}O_{24}$ and $Ba_8Ta_4Ru_{8/3}Zn_{2/3}O_{24}$. Solid lines denote the fits to Eq. (1).

(in $Ba_8Ta_4Ru_{8/3}Zn_{2/3}O_{24}$) and $Ru^{4+}(Co^{2+})$–O–$Ru^{4+}(Co^{2+})$ (in $Ba_8Ta_4Ru_{8/3}Co_{2/3}O_{24}$) fluctuations persist. Nevertheless, no clear magnetic transition could be detected, in agreement with the TOF neutron diffraction data, which evidenced random distribution of Ru and Co atoms and location of vacancies in 4*e* and 8*h* sites (see below). The effective magnetic moment, $\mu_{eff} = \sqrt{8C}$, deduced from the Curie constant for $Ba_8Ta_4Ru_{8/3}Zn_{2/3}O_{24}$ is 1.58 μ_B (μ_B: Bohr magnetron) per Ru ion. The formal oxidation state of Ru atoms in these compounds is +4. The magnetic moment of Ru^{4+} ($S = 1$) was calculated at 2.828 μ_B, on the assumption of a low-spin state and a zero-angular momentum. The latter value is considerably larger than the experimental effective magnetic moment. It is well known that in palladium and platinum group ions, the total angular momentum quantum number J can still be employed even in the presence of a crystal field. When the angular momentum of Ru ions survives in the crystal field, the effective magnetic moment may be reduced from the spin only moment. Small experimental magnetic moments have been reported for 4*d* and 5*d* transition metal ions [33]. If we assume that $Ba_8Ta_4Ru_{8/3}Zn_{2/3}O_{24}$ and $Ba_8Ta_4Ru_{8/3}Co_{2/3}O_{24}$ have the same $\mu_{eff}(Ru^{4+})$, $\mu_{eff}(Co^{2+})$ in $Ba_8Ta_4Ru_{8/3}Co_{2/3}O_{24}$ can be calculated using the following equation:

$$3\mu_{eff}^2 = 8\mu_{eff}^2(Ru^{4+}) + 2\mu_{eff}^2(Co^{2+}). \quad (2)$$

μ_{eff} for $Ba_8Ta_4Ru_{8/3}Co_{2/3}O_{24}$, deduced from the Curie constant, is 4.20 μ_B per formula unit. From these data, one can obtain $\mu_{eff}(Co^{2+}) = 4.06\,\mu_B$. This value lies between the theoretical value, 3.87 μ_B, which is expected for the free Co^{2+} ion, and 4.8 μ_B, usually observed for Co^{2+} ions [34].

Fig. 2 shows selected-area ED patterns along [0001], [10$\bar{1}$0] and [$\bar{2}$110] zones for $Ba_8Ta_4Ru_{8/3}Co_{2/3}O_{24}$. The brightest reflections on the ED patterns correspond to a sublattice with lattice parameters $a_{sub} \approx 5.7$ Å and $c_{sub} \approx 18.9$ Å. The [$\bar{2}$110] diffraction pattern is very similar to those reported for $Ba_8Ta_4Ti_3O_{24}$ and $Ba_8Ta_6NiO_{24}$ [22,23] and exhibits superstructure spots which can be indexed in a hexagonal system with lattice parameters $a \approx 10.0$ Å and $c \approx 18.9$ Å. It corresponds to the superstructure $a = \sqrt{3} \times a_{sub}$ and to a rotation of 30° around the crystallographic *c*-axis. The [$\bar{2}$110] diffraction pattern shows the reflection conditions of $l = 2n$ for $0\,0\,0\,l$ and $0\,h\,\bar{h}\,l$. The space group with the highest symmetry in agreement with this condition is $P6_3/mcm$. The presence of the $0\,0\,0\,l$ reflections with $l = 2n + 1$ in the [10$\bar{1}$0] diffraction pattern is due to double diffraction from the $h\,\overline{2h}\,h\,l$ rows. In contrast to $Ba_8Ta_4Ti_3O_{24}$ and $Ba_8Ta_6NiO_{24}$, the $0\,1\,\bar{1}\,0$, $0\,2\,\bar{2}\,0$, and equivalent reflections were absent in the [0001] diffraction pattern of $Ba_8Ta_4Ru_{8/3}Co_{2/3}O_{24}$. The presence of the $0\,1\,\bar{1}\,0$ and $0\,2\,\bar{2}\,0$ reflections on the [$\bar{2}$110] diffraction pattern should thus be attributed to double diffraction.

First, we refined structure parameters of $Ba_8Ta_4Ru_{8/3}Co_{2/3}O_{24}$ from the TOF neutron powder diffraction data in the sublattice model in space group $P6_3/mmc$ using fractional coordinates of $Ba_8Ta_4Ti_3O_{24}$ [22] as the initial ones. This refinement afforded lattice parameters of $a = 5.77792(4)$ Å and $c = 18.9251(2)$ Å ($Z = 1$) and *R* factors of $R_{wp} = 4.70\%$ ($S = 1.63$), $R_p = 3.91\%$, $R_B = 3.46\%$, and $R_F = 2.25\%$. This model has one site (*M*: 4*e*) with fixed occupancies, $g(Ru) = 2/3$ and $g(Co) = 1/6$, as follows from the total chemical composition. The refined thermal parameter $U(M)$ was equal to $2.8(6) \times 10^{-3}$ Å^2.

Taking into account the superstructure observed by ED, we transformed the obtained structure parameters to those in space group $P6_3/mcm$ with $a = \sqrt{3} \times a_{sub}$ and $c = c_{sub}$. Because actually no superstructure reflections were observed on the experimental TOF neutron diffraction patterns and also on the XRD patterns, we had to impose some linear constraints on the structure parameters to make the refinement in the superstructure model successful. These constraints were $U(Ba1) = U(Ba2)$, $U(M1) = U(M2)$, $U(O1) = U(O2)$, and $U(O5) = U(O6)$. Note that each pair of these atoms in the superstructure model is one and the same atom in the substructure model.

When only Ru atoms were placed at the *M*1 and *M*2 sites, the refinement resulted in $g(Ru) = 0.83(6)$ for the *M*1 site and $g(Ru) = 0.72(3)$ for the *M*2 site with $U(M1) = U(M2) = 3(7) \times 10^{-4}$ Å^2. This fact indicated that the *M*1 and *M*2 sites had slightly different

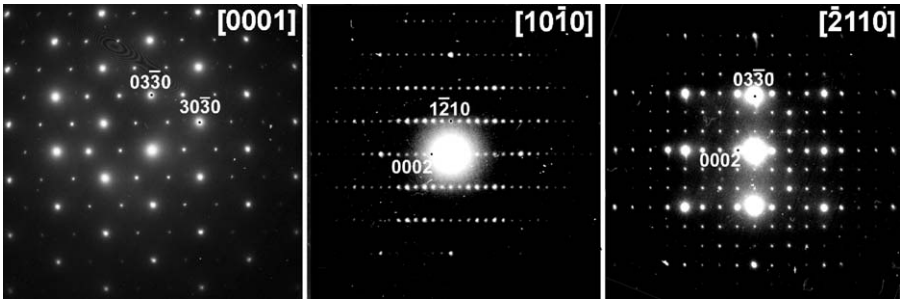

Fig. 2. Selected-area ED patterns of $Ba_8Ta_4Ru_{8/3}Co_{2/3}O_{24}$ along the [0001], [10$\bar{1}$0] and [$\bar{2}$110] directions (from left to right). Superstructure spots are seen in the [$\bar{2}$110] zone but absent in the [0001] zone.

occupation factors. Because b_c for Co is about 3 times smaller than that for Ru, it was very difficult to refine the distribution of Co atoms between the $M1$ and $M2$ sites. We assumed $g(\mathrm{Co}) = 1/6$ for the $M1$ and $M2$ sites as follows from the substructure model. We refined only distribution of Ru atoms between the $M1$ and $M2$ sites with the constraint on the total chemical composition, i.e., $g_{M2}(\mathrm{Ru}) = 1 - 0.5 g_{M1}(\mathrm{Ru})$. Note that we checked models with different distribution of Ru and Co atoms between the $M1$ and $M2$ sites. However, these models did not improve the fit and in some cases led to negative thermal parameters for the $M1$ ($M2$) site.

For the impurity phase, $Ba_3CoRu_2O_9$, only a scale factor and lattice parameters were refined. Profile parameters of $Ba_3CoRu_2O_9$ were constrained to be equal to those of $Ba_8Ta_4Ru_{8/3}Co_{2/3}O_{24}$. We excluded diffraction data in a d range of 2.259–2.311 Å containing reflections of an unknown impurity from the Rietveld refinement.

The subsequent Rietveld analyses afforded sufficiently low R factors and reasonable U parameters for all the sites. Partial profile relaxation [35] was applied to 225, 226, and 600 reflections to improve their fits at the last stage of the structure refinement.

Table 1 lists experimental and refinement conditions, lattice parameters, R factors, and so forth. Fractional coordinates and U parameters for the final Rietveld analysis appear in Table 2, and selected interatomic distances calculated with ORFFE [36] in Table 3. Numbers in parentheses are estimated standard deviations of the last significant digits throughout this paper. Fig. 3 displays observed, calculated, and difference TOF neutron diffraction patterns for $Ba_8Ta_4Ru_{8/3}Co_{2/3}O_{24}$.

Table 1
Conditions of the TOF neutron powder diffraction experiment and part of refinement results for $Ba_8Ta_4Ru_{8/3}Co_{2/3}O_{24}$

No. of data points	6177
d (Å)	0.45–2.5
Space group	$P6_3/mcm$ (no. 193)
a (Å)	10.0075(1)
c (Å)	18.9248(2)
V (Å^3)	1641.38(4)
Z	3
No. of Bragg reflections	3400
Variables	
Structure/lattice parameters	26/2
Background/profile parameters	15/16
R_{wp}, R_p	4.60%, 3.85%
R_B, R_F	3.21%[a], 1.86%[b]; 2,62%[a], 1.80%[b]
S	1.60[c]

[a] For $Ba_8Ta_4Ru_{8/3}Co_{2/3}O_{24}$ (97.6 mass%).
[b] For $Ba_3CoRu_2O_9$ (2.4 mass%).
[c] $S = R_{wp}/R_e$.

Table 2
Fractional coordinates and isotropic atomic displacement parameters for $Ba_8Ta_4Ru_{8/3}Co_{2/3}O_{24}$

Atom	Wyckoff position	x	y	z	10^2U (Å^2)
Ba1	2b	0	0	0	0.55(7)
Ba2	4d	1/3	2/3	0	= U(Ba1)
Ba3	6g	0.337(4)	0	1/4	0.31(9)
Ba4	12k	0.669(3)	0	0.1364(2)	0.58(5)
Ta	12k	0.666(2)	0	0.56201(14)	0.19(3)
$M1$	4e	0	0	0.1820(11)	0.06(5)
$M2$	8h	1/3	2/3	0.1860(7)	= U($M1$)
O1	6g	0.840(4)	0	1/4	0.79(4)
O2	12j	0.669(4)	0.174(3)	1/4	= U(O1)
O3	12k	0.173(2)	0	0.1241(6)	0.73(16)
O4	24e	0.4979(10)	0.1620(14)	0.3810(3)	0.26(6)
O5	6f	1/2	0	0	0.77(3)
O6	12i	0.167(2)	2x	0	= U(O5)

Note: $g(\mathrm{Ru}) = 0.76(7)$ and $g(\mathrm{Co}) = 1/6$ for the $M1$ site and $g(\mathrm{Ru}) = 0.62(7)$ and $g(\mathrm{Co}) = 1/6$ for the $M2$ site. The occupancies of all the other sites are unity.

Table 3
Selected interatomic distances (Å) in $Ba_8Ta_4Ru_{8/3}Co_{2/3}O_{24}$

Ba1–O3 (× 6)	2.92(1)
Ba1–O6 (× 6)	2.89(3)
Ba2–O4 (× 6)	2.822(6)
Ba2–O5 (× 3)	2.8889(1)
Ba2–O6 (× 3)	2.89(3)
Ba3–O1 (× 2)	2.92(4)
Ba3–O2 (× 2)	2.87(3)
Ba3–O2 (× 2)	2.88(5)
Ba3–O3 (× 2)	2.89(3)
Ba3–O4 (× 4)	2.96(1)
Ba4–O1	2.75(3)
Ba4–O2 (× 2)	2.77(2)
Ba4–O3 (× 2)	2.88(3)
Ba4–O4 (× 2)	2.91(3)
Ba4–O4 (× 2)	2.93(2)
Ba4–O5	3.09(2)
Ba4–O6 (× 2)	3.067(9)
$M1$–O1 (× 3)	2.05(3)
$M1$–O3 (× 3)	2.05(2)
$M1$–$M1'$	2.57(4)
$M2$–O2 (× 3)	2.01(2)
$M2$–O4 (× 3)	2.12(1)
$M2$–$M2'$	2.42(3)
Ta–O3	2.00(2)
Ta–O4 (× 2)	1.96(1)
Ta–O5	2.04(2)
Ta–O6 (× 2)	2.041(8)

The calculated ED patterns based on this model are in agreement with the experimental patterns. Calculation of the intensities (using MacTempas software) of the $0\,1\,\bar{1}\,0$ and $0\,2\,\bar{2}\,0$ reflections on the basis of this model showed that these reflections indeed had intensities very near to zero.

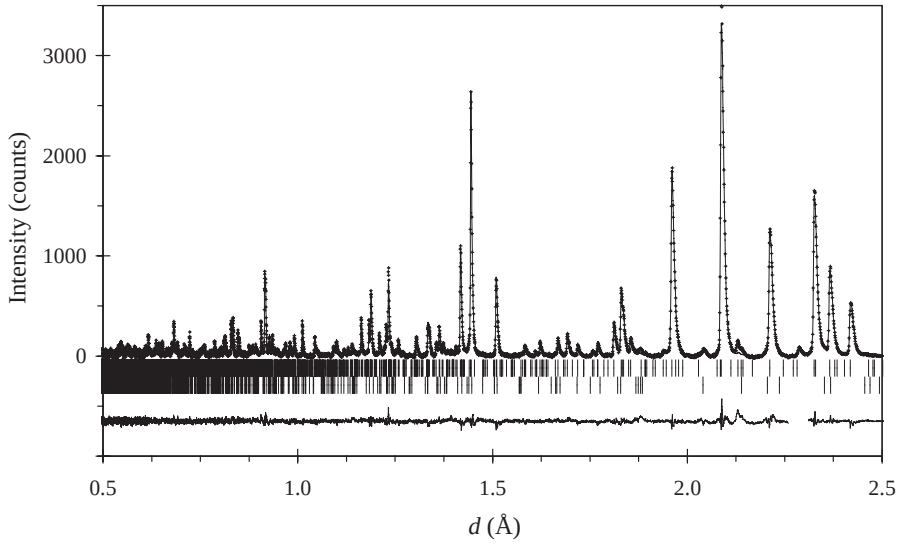

Fig. 3. Observed (crosses), calculated (solid line), and difference patterns resulting from the Rietveld analysis of the TOF neutron powder diffraction data for $Ba_8Ta_4Ru_{8/3}Co_{2/3}O_{24}$. Bragg reflections for $Ba_8Ta_4Ru_{8/3}Co_{2/3}O_{24}$ (upper) and $Ba_3CoRu_2O_9$ (lower) are indicated by tick marks. Background intensities were subtracted from the observed and calculated TOF neutron diffraction patterns.

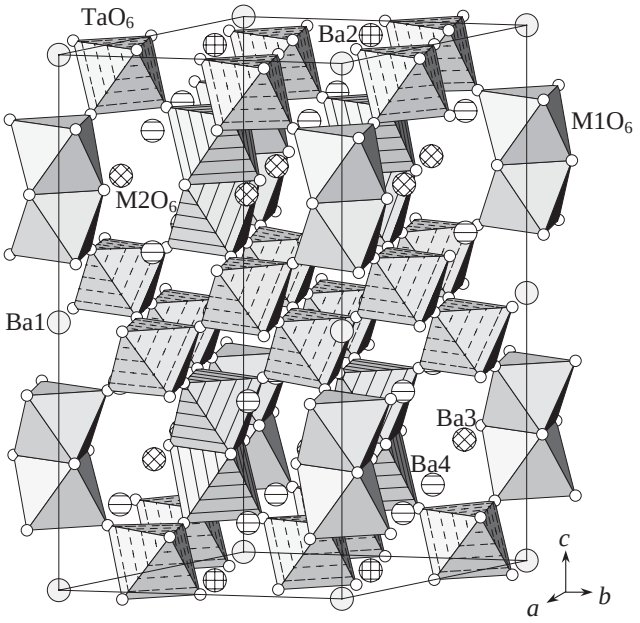

Fig. 4. Crystal structure of $Ba_8Ta_4Ru_{8/3}Co_{2/3}O_{24}$.

4. Discussion

Fig. 4 shows the crystal structure of $Ba_8Ta_4Ru_{8/3}Co_{2/3}O_{24}$. This phase is a representative of the B-cation deficient $A_nB_{n-1}O_{3n}$ ($n = 8$) series of perovskite-type compounds with ($hc\ldots c$) sequence. Its structure consists of 8H $(cchc)_2$ or ABCBACBC stacking of BaO_3 close-packed layers and can be described as an alternation of two FSO and two CSO fragments. The cation sum in the B-framework differs from 7 in $Ba_8Ta_4Ru_{8/3}Co_{2/3}O_{24}$ because of the lower average oxidation state. As a result, the total occupation factor of the cation positions in FSO (83.3%) is slightly higher than that in the other related compounds (e.g., $Ba_8Ta_4Ti_3O_{24}$ and $Ba_8Ta_6NiO_{24}$).

In the present structural model for $Ba_8Ta_4Ru_{8/3}Co_{2/3}O_{24}$ with space group $P6_3/mcm$, there are two pairs of FSO partially occupied by Ru and Co. Ta^{5+} ions with a high formal oxidation state fully occupy the site in CSO. This cation distribution favors a decrease in strong electrostatic repulsion in FSO. The average metal–oxygen distance in FSO is 2.06 Å and slightly larger than the Ru–O distance in $Ba_3CoRu_2O_9$ (1.977 Å), which is ascribed to the lower oxidation state of Ru in $Ba_8Ta_4Ru_{8/3}Co_{2/3}O_{24}$ (+4) and the presence of vacancies at this site.

The ionic radii of Ru^{4+} (0.62 Å) and Ta^{5+} (0.64 Å) for 6-fold coordination [37] are very close to each other, which may lead to disordering of these ions. Because the b_c's for Ru and Ta are very close to each other, we checked the possibility of the disorder of Ru and Ta atoms using the XRD data. The XRD data also did not give any evidence for the disordering of Ru and Ta atoms, which is explained in terms of a well-known tendency of Ru to form metal–metal bonds. Ru occupies (together with Co) the sites in the FSO layers to realize the direct Ru–Ru interaction. The average $M1(2)$–$M1(2)$ distance is 2.495 Å, which is smaller than the corresponding distance in $Ba_8Nb_4Ti_3O_{24}$ (2.64 Å; $g(Nb) = 0.24$ and $g(Ti) = 0.635$) [24] and approximately equal to that in $Ba_8Ta_4Ti_3O_{24}$ (2.48 Å; $g(Ta) = 0.25$ and $g(Ti) = 0.625$) [22]. It was difficult to refine the Co distribution between the $M1$ and $M2$ sites due its small b_c value. Single crystal X-ray diffraction data are required to investigate the cation distribution in FSO in details as it was performed for $Ba_8Nb_4Ti_3O_{24}$ [24]. In

contrast with $Ba_8Ti_3Nb_4O_{24}$, there is no cation disorder in CSO in $Ba_8Ta_4Ru_{8/3}Co_{2/3}O_{24}$. CSO are occupied only by Ta. The Ta–O distances are close to each other and the average value is 2.007 Å. Ba^{2+} cations are in the typical 12-fold coordination.

Low-temperature antiferromagnetic ordering was observed in 6H perovskite-type compounds $Ba_3MRu_2O_9$ (M = Co and Ni) [27]. However, we did not find any evidence for magnetic ordering down to 5 K in $Ba_8Ta_4Ru_{8/3}Co_{2/3}O_{24}$ and $Ba_8Ta_4Ru_{8/3}Zn_{2/3}O_{24}$. $Ba_8Ta_4Ru_{8/3}Co_{2/3}O_{24}$ and $Ba_3MRu_2O_9$ (M = Co and Ni) have different cation distributions. In $Ba_3MRu_2O_9$, M^{2+} and Ru^{5+} ions are completely ordered and occupy positions in CSO and FSO, respectively. Another difference between $Ba_3MRu_2O_9$ and $Ba_8Ta_4Ru_{8/3}Co_{2/3}O_{24}$ is found in the distances between the centers of FSO. The Ru–Ru distance in $Ba_3CoRu_2O_9$ was found to be 2.684 Å, which is much larger than that in $Ba_8Ta_4Ru_{8/3}Co_{2/3}O_{24}$ (see Table 3). One can conclude that the absence of complete ordering of Ru and Co atoms between the $M1$ and $M2$ sites and the shorter metal−metal distances in FSO may be a reason of magnetic order suppression.

5. Conclusions

The three new B-deficient perovskite-type oxides, $Ba_8Ta_4Ru_{8/3}M_{2/3}O_{24}$ (M = Co, Ni and Zn), have been synthesized. The crystal structure of $Ba_8Ta_4Ru_{8/3}Co_{2/3}O_{24}$ was found to be similar to those of $Ba_8Ta_4Ti_3O_{24}$, $Ba_8Nb_4Ti_3O_{24}$, and $Ba_8Ta_6NiO_{24}$. Ta and Ru/Co atoms are located exclusively at the 12k and 4e/8h sites, respectively. Statistical occupation of the 4e and 8h sites by Ru, Co, and vacancies results in suppression of the magnetic order.

Acknowledgments

The authors would like to thank Professor T. Kamiyama for his help in the TOF neutron data collection and Professor G. Van Tendeloo for the interesting discussion. This work was supported by the Multi-Core Project and Special Coordination Funds of the Science and Technology Agency of the Japanese Government and in part by the program IAP V-1 of the Belgian Government.

References

[1] P.C. Donohue, L. Katz, R. Ward, Inorg. Chem. 43 (1965) 306.
[2] A.M. Abakumov, E.V. Antipov, L.M. Kovba, E.M. Kopnin, S.N. Putilin, R.V. Shpanchenko, Russ. Chem. Rev. 64 (1995) 769 (and references therein).
[3] P.D. Battle, S.H. Kim, A.V. Powell, J. Solid State Chem. 101 (1992) 161.
[4] F. Galasso, L. Katz, Acta Crystallogr. 14 (1961) 647.
[5] C. Calvo, H.N. Ng, B.L. Chamberland, Inorg. Chem. 17 (1978) 699.
[6] J. Shannon, L. Katz, Acta Crystallogr. B 26 (1970) 102.
[7] W. Wischert, H.-J. Schittenhelm, S. Kemmler-Sack, Z. Anorg. Allg. Chem. 448 (1979) 119.
[8] H.-J. Roter, S. Kemmler-Sack, U. Treiber, W.-R. Cyris, Z. Anorg. Allg. Chem. 466 (1980) 131.
[9] M. Hermann, L.M. Kovba, Russ. J. Inorg. Chem. 28 (1983) 2377.
[10] M. Hermann, L.M. Kovba, Russ. J. Inorg. Chem. 30 (1985) 317.
[11] H.C. van Duivenboden, H.W. Zandbergen, D.J.W. Ijdo, Acta Crystallogr. C 42 (1986) 266.
[12] B. Mössner, S. Kemmler-Sack, J. Less-Common Met. 120 (1986) 203.
[13] R. Bonchev, F. Weill, J. Darriet, Mater. Res. Bull. 27 (1992) 931.
[14] R. Bontchev, B. Darriet, J. Darriet, F. Weill, G. Van Tendeloo, S. Amelinckx, Eur. J. Solid State Inorg. Chem. 30 (1993) 521.
[15] G. Van Tendeloo, S. Amelinckx, B. Darriet, R. Bontchev, J. Darriet, F. Weill, J. Solid State Chem. 108 (1994) 314.
[16] A.M. Abakumov, R.V. Shpanchenko, E.V. Antipov, O.I. Lebedev, G. Van Tendeloo, S. Amelinckx, J. Solid State Chem. 141 (1998) 492.
[17] N. Harre, D. Mercurio, G. Troilliard, B. Frit, Mater. Res. Bull. 10 (1998) 1537.
[18] G. Trolliard, N. Harre, D. Mercurio, B. Frit, J. Solid State Chem. 145 (1999) 678.
[19] N. Teneze, D. Mercurio, G. Troilliard, B. Frit, Mater. Res. Bull. 35 (2000) 1603.
[20] G. Troilliard, N. Teneze, Ph. Boullay, M. Manier, D. Mercurio, J. Solid State Chem. 173 (2003) 91.
[21] Ph. Boullay, N. Teneze, G. Troillard, D. Mercurio, J.M. Perez-Mato, J. Solid State Chem. 174 (2003) 209.
[22] R.V. Shpanchenko, L. Nistor, G. Van Tendeloo, J. Van Landuyt, S. Amelinckx, A.M. Abakumov, E.V. Antipov, L.M. Kovba, J. Solid State Chem. 114 (1995) 560.
[23] A.M. Abakumov, G. Van Tendeloo, A.A. Scheglov, R.V. Shpanchenko, E.V. Antipov, J. Solid State Chem. 125 (1996) 102.
[24] N. Teneze, P. Boullay, V. Petricek, G. Trolliard, D. Mercurio, Solid State Sci. 4 (2002) 1129.
[25] C. Renard, S. Daviero-Minaud, M. Huvé, F. Abraham, J. Solid State Chem. 144 (1999) 125.
[26] A.J. Yacobson, B.M. Collins, B.E.F. Fender, Acta Crystallogr. B 32 (1976) 1083.
[27] P. Lightfoot, P.D. Battle, J. Solid State Chem. 89 (1990) 174.
[28] J.T. Rijssenbeek, P.M. Atl, B. Batlogg, N.P. Ong, R.J. Cava, Phys. Rev. B 58 (1996) 10315.
[29] M. Bieringer, S.M. Moussa, L.D. Noailles, A. Burrows, C.J. Kiely, M.J. Rosseinsky, R.M. Ibberson, Chem. Mater. 15 (2003) 586.
[30] E. Quarez, M. Huvé, F. Abraham, O. Mentré, Solid State Sci. 5 (2003) 951.
[31] T. Ohta, F. Izumi, K. Oikawa, T. Kamiyama, Physica B 234–236 (1997) 1093.
[32] V.F. Sears, International Tables for Crystallography, Vol. C, 2nd Edition, Kluwer, Dordrecht, 1999, pp. 440–450.
[33] J.H. Van Vleck, in: The Theory of Electric and Magnetic Susceptibility, Oxford University Press, Oxford, 1965, p. 312.
[34] C. Kittel, Introduction to Solid State Physics, 6th Edition, Wiley, New York, 1986, p. 406.
[35] F. Izumi, T. Ikeda, Mater. Sci. Forum 321–324 (2000) 198.
[36] W.R. Busing, K.O. Martin, H.A. Levy, Report ORNL-TM-306, Oak Ridge National Laboratory, Tennessee, 1964.
[37] R.D. Shannon, Acta Crystallogr. A 32 (1976) 751.